Report. Optically stimulated luminescence profiling and dating of cores TP22-VC03, TP22-VC07 and TP22-VC026

Tim Kinnaird
School of Earth and Environmental Sciences, University of St Andrews

Soetkin Vervust
Archaeology, Environmental Changes, and Geo-Chemistry (AMGC), Vrije Universiteit Brussel

Víctor Cartelle, Ruth Plets
Flanders Marine Institute (VLIZ)

Introduction

This supplementary data file concerns the optically stimulated luminescence investigations of cores TP22-VC03, TP22-VC07 and TP22-VC26.

Methodology

We utilised a three-stage approach of optically stimulated luminescence profiling and dating (OSL-PD), to appraise the sediment recovered in core from TP22-VC03, TP22-VC07 and TP22-VC26. First, the luminescence properties of bulk sediment sampled directly from core were appraised using portable OSL equipment. This proxy information was used to construct relative luminescence stratigraphies for each core (OSL signal intensities vs depth; figures S1 to S3) and select the most promising positions for dating. Then, a subset of these profiling samples was progressed to calibrated luminescence screening and characterisation in the laboratory, stage 2, to provide a first approximation in the magnitude and range in apparent doses (OSL apparent doses vs depth; figures S1 to S3). Finally, those samples that have significance for interpreting the depositional histories of TP22-VC03, TP22-VC07 and TP22-VC26, coupled with promising attributes in stages 1 and 2, were progressed to dating (stage 3).

Stage 1: Sample collection and profiling

Tim Kinnaird visited VLIZ between the 26th and 28th of January 2023 to sample cores TP22-VC03, TP22-VC07 and TP22-VC26 for OSL-PD. The sediment recovered in core was sampled at ~5-10 cm intervals, with closer resolution sampling across stratigraphic boundaries. 27 samples were taken from TP22-VC03, 23 from TP22-VC07 and 27 from TP22-VC26. Initial screening results using portable OSL equipment (Munyikwa et al., 2021) provided near real-time information on luminescence signal progressions and breaks down core and suggest hypotheses on depositional histories and correlations. The progressions and breaks in OSL net signal intensities down-core are shown in figures S1 to S3 (left-hand plots) and are tabulated in table S1.

Stage 2: OSL screening and sample selection

Sample preparation protocols as previously utilised in the luminescence laboratories at School of Earth and Environmental Sciences, University of St Andrews (cf. Turner et al., 2021; Lichtenberger et al., 2019) were used to obtain HF-etched quartz, which was dispensed to disc in duplicate, and subjected to a simplified single-aliquot regenerative dose (SAR) OSL protocol (cf. Turner et al., 2021; Vervust et al. 2020).

OSL measurements were carried out using Risø TL/OSL DA-20 automated dating systems. The readout cycles comprised a natural readout, followed by a nominal 1Gy test dose, then regenerative doses of either ~1.0, 2.4, 4.8 and 19.1 Gy (TP22-VC07 and TP22-VC26) or ~5.4, 10.7, 32.1 and 64.2 Gy (TP22-VC03), and a further 1Gy test dose. The readout cycle also included a zero dose, a repeat dose (equivalent to the first regenerative dose) and an IRSL dose. A 220˚C preheat held for 10s was used with 60s OSL measurements using the blue LEDs. Test doses were preheated at the same temperature has the preceding measurement and held for the same duration.

This provided the first, preliminary assessment of luminescence sensitivities (luminescence per unit dose, counts Gy^{-1}) and apparent dose estimates (Gy) throughout the sampled stratigraphies. The distributions in apparent dose down-core are shown in figures S1 to S3 (right-hand plots) and are tabulated in table S2. The term apparent dose is used here, to distinguish these values from the equivalent doses that are reported later.

Table S1: IRSL and OSL net signal intensities, IRSL and OSL depletion indices and the IRSL: OSL ratio for cores TP22-VC03, TP22-VC07 and TP22-VC26 ('-', not measured)

Sample ID	Depth / cm	IRSL		OSL		IRSL : OSL ratio
		net signal intensities / counts	Depletion ratio	net signal intensities / counts	Depletion ratio	
TP22 VC03-1	5	-	-	2290 ± 60	1.34 ± 0.06	-
TP22 VC03-2	16	920 ± 40	1.18 ± 0.09	9860 ± 100	1.64 ± 0.03	0.0933 ± 0.0046
TP22 VC03-3	28	-	-	5800 ± 90	1.68 ± 0.05	-
TP22 VC03-4	39	270 ± 40	1.32 ± 0.16	2900 ± 60	1.64 ± 0.07	0.0929 ± 0.0132
TP22 VC03-5	48	590 ± 40	1.41 ± 0.13	5200 ± 80	1.57 ± 0.05	0.1130 ± 0.0079
TP22 VC03-6	58	2050 ± 50	1.03 ± 0.18	3390 ± 70	1.51 ± 0.06	0.6038 ± 0.0196
TP22 VC03-7	68	4830 ± 80	1.17 ± 0.04	46700 ± 220	1.66 ± 0.02	0.1035 ± 0.0017
TP22 VC03-8	78	1330 ± 50	1.36 ± 0.09	10830 ± 110	1.80 ± 0.04	0.1228 ± 0.0046
TP22 VC03-9	88	310 ± 30	0.91 ± 0.12	2080 ± 60	1.63 ± 0.08	0.1488 ± 0.0171
TP22 VC03-10	98	3230 ± 70	1.23 ± 0.05	20840 ± 150	1.77 ± 0.03	0.1548 ± 0.0033
TP22 VC03-11	108	360 ± 40	1.29 ± 0.16	4340 ± 70	1.62 ± 0.05	0.0830 ± 0.0085
TP22 VC03-12	118	290 ± 40	2.57 ± 0.33	3360 ± 70	1.52 ± 0.06	0.0861 ± 0.0112
TP22 VC03-13	127	1670 ± 50	1.41 ± 0.08	14810 ± 130	1.56 ± 0.03	0.1130 ± 0.0036
TP22 VC03-14	137	290 ± 30	1.07 ± 0.14	3160 ± 60	1.65 ± 0.06	0.0905 ± 0.0111
TP22 VC03-15	141	13630 ± 120	1.27 ± 0.02	156240 ± 400	1.57 ± 0.01	0.0872 ± 0.0008
TP22 VC03-16	148	23180 ± 160	1.27 ± 0.02	320480 ± 570	1.54 ± 0.01	0.0723 ± 0.0005
TP22 VC03-17	154	69670 ± 270	1.23 ± 0.01	844270 ± 920	1.72 ± 0.01	0.0825 ± 0.0003
TP22 VC03-18	162	95530 ± 310	1.22 ± 0.01	1231500 ± 1110	1.72 ± 0.01	0.0776 ± 0.0003
TP22 VC03-19	170	606790 ± 780	1.25 ± 0.01	6173740 ± 2490	1.77 ± 0.01	0.0983 ± 0.0001
TP22 VC03-20	177	1302800 ± 1150	1.28 ± 0.01	11398010 ± 3390	1.91 ± 0.01	0.1143 ± 0.0001
TP22 VC03-21	187.5	1415830 ± 1200	1.27 ± 0.01	12001190 ± 3470	1.92 ± 0.01	0.1180 ± 0.0001
TP22 VC03-22	194.5	493270 ± 710	1.27 ± 0.01	5075200 ± 2260	1.92 ± 0.01	0.0972 ± 0.0001
TP22 VC03-23	200.5	489900 ± 700	1.25 ± 0.01	5200860 ± 2290	1.79 ± 0.01	0.0942 ± 0.0001
TP22 VC03-24	208.5	941900 ± 970	1.29 ± 0.01	8762360 ± 2970	1.89 ± 0.01	0.1075 ± 0.0001
TP22 VC03-25	217.5	1172330 ± 1090	1.25 ± 0.01	12116280 ± 3490	1.79 ± 0.01	0.0968 ± 0.0001
TP22 VC03-26	224.5	764780 ± 880	1.18 ± 0.01	7991700 ± 2830	1.91 ± 0.01	0.0957 ± 0.0001
TP22 VC03-27	232.5	743750 ± 870	1.28 ± 0.01	7363760 ± 2720	1.90 ± 0.01	0.1010 ± 0.0001
TP22 VC07-1	10	700 ± 40	1.24 ± 0.11	20890 ± 150	1.24 ± 0.02	0.0336 ± 0.0021
TP22 VC07-2	17	6640 ± 90	1.05 ± 0.13	24320 ± 160	1.36 ± 0.02	0.2728 ± 0.004
TP22 VC07-3	23.5	5760 ± 80	1.37 ± 0.04	72680 ± 270	1.96 ± 0.02	0.0793 ± 0.0012
TP22 VC07-4	33.5	10540 ± 110	1.34 ± 0.03	102530 ± 320	1.85 ± 0.01	0.1028 ± 0.0011
TP22 VC07-5	43.5	7520 ± 90	1.32 ± 0.03	90010 ± 300	1.99 ± 0.01	0.0835 ± 0.0011
TP22 VC07-6	52.5	6870 ± 90	1.31 ± 0.03	69670 ± 270	1.79 ± 0.01	0.0986 ± 0.0013
TP22 VC07-7	63.5	6370 ± 90	1.36 ± 0.04	79270 ± 280	1.82 ± 0.01	0.0803 ± 0.0011
TP22 VC07-8	73.5	7540 ± 90	1.29 ± 0.03	70600 ± 270	1.81 ± 0.01	0.1067 ± 0.0014
TP22 VC07-9	83.5	20530 ± 150	1.24 ± 0.03	112350 ± 340	2.00 ± 0.01	0.1827 ± 0.0014
TP22 VC07-10	93.5	7100 ± 90	1.30 ± 0.03	101410 ± 320	2.21 ± 0.02	0.0700 ± 0.0009
TP22 VC07-11	103.5	5000 ± 80	1.32 ± 0.04	70030 ± 270	1.83 ± 0.01	0.0713 ± 0.0011
TP22 VC07-12	112.5	6440 ± 90	1.30 ± 0.03	62130 ± 250	1.80 ± 0.02	0.1036 ± 0.0015
TP22 VC07-13	116.5	7850 ± 90	1.27 ± 0.03	77560 ± 280	1.76 ± 0.01	0.1012 ± 0.0013
TP22 VC07-14	125	12530 ± 120	1.42 ± 0.03	113340 ± 340	1.91 ± 0.01	0.1105 ± 0.0011
TP22 VC07-15	134	9130 ± 100	1.38 ± 0.03	82860 ± 290	1.90 ± 0.01	0.1102 ± 0.0013
TP22 VC07-16	144	6940 ± 90	1.31 ± 0.03	70040 ± 270	1.89 ± 0.02	0.0991 ± 0.0013
TP22 VC07-17	154	7870 ± 100	1.31 ± 0.03	82020 ± 290	1.81 ± 0.01	0.0959 ± 0.0012
TP22 VC07-18	164	11610 ± 110	1.30 ± 0.02	115770 ± 340	1.89 ± 0.01	0.1003 ± 0.0010

TP22 VC07-19	174	8910 ± 100	1.33 ± 0.03	94880 ± 310	1.87 ± 0.01	0.0939 ± 0.0011
TP22 VC07-20	184	12040 ± 120	1.28 ± 0.02	119490 ± 350	1.94 ± 0.01	0.1007 ± 0.0010
TP22 VC07-21	194	11750 ± 110	1.34 ± 0.03	106570 ± 330	1.85 ± 0.01	0.1103 ± 0.0011
TP22 VC07-22	204	8050 ± 90	1.30 ± 0.03	84250 ± 290	1.90 ± 0.01	0.0955 ± 0.0012
TP22 VC07-23	209	8080 ± 100	1.31 ± 0.03	81010 ± 290	1.90 ± 0.01	0.0998 ± 0.0012
TP22 VC026-1	10	-	-	13390 ± 120	1.29 ± 0.02	-
TP22 VC026-2	19	-	-	30810 ± 180	1.45 ± 0.02	-
TP22 VC026-3	27.5	-	-	114310 ± 340	1.78 ± 0.01	-
TP22 VC026-4	35.5	-	-	112980 ± 340	1.78 ± 0.01	-
TP22 VC026-5	42.5	-	-	157110 ± 400	1.80 ± 0.01	-
TP22 VC026-6	50.5	9490 ± 100	1.26 ± 0.03	124800 ± 360	1.76 ± 0.01	0.0760 ± 0.0009
TP22 VC026-7	56.5	11720 ± 110	1.27 ± 0.02	155620 ± 400	1.84 ± 0.01	0.0753 ± 0.0007
TP22 VC026-8	61.5	5920 ± 80	1.3 ± 0.04	79330 ± 280	1.75 ± 0.01	0.0746 ± 0.0011
TP22 VC026-9	70.5	12740 ± 120	1.28 ± 0.02	150870 ± 390	1.74 ± 0.01	0.0845 ± 0.0008
TP22 VC026-10	80.5	13700 ± 120	1.32 ± 0.02	176880 ± 420	1.78 ± 0.01	0.0775 ± 0.0007
TP22 VC026-11	90.5	11610 ± 110	1.32 ± 0.03	146640 ± 380	1.78 ± 0.01	0.0792 ± 0.0008
TP22 VC026-12	100.5	14010 ± 120	1.25 ± 0.02	158460 ± 400	1.62 ± 0.01	0.0884 ± 0.0008
TP22 VC026-13	110.5	6070 ± 80	1.23 ± 0.03	81700 ± 290	1.78 ± 0.01	0.0743 ± 0.0011
TP22 VC026-14	117.5	8270 ± 100	1.31 ± 0.03	119420 ± 350	1.65 ± 0.01	0.0692 ± 0.0008
TP22 VC026-15	123	4200 ± 70	1.17 ± 0.04	83840 ± 290	1.48 ± 0.01	0.0501 ± 0.0009
TP22 VC026-16	129	15370 ± 130	1.24 ± 0.02	209680 ± 460	1.60 ± 0.01	0.0733 ± 0.0006
TP22 VC026-17	133	6880 ± 90	1.25 ± 0.03	141170 ± 380	1.40 ± 0.01	0.0488 ± 0.0006
TP22 VC026-18	139	6100 ± 80	1.26 ± 0.03	123580 ± 350	1.35 ± 0.01	0.0494 ± 0.0007
TP22 VC026-19	150	-	-	-	-	-
TP22 VC026-20	158	-	-	273950 ± 530	1.30 ± 0.01	-
TP22 VC026-21	166	-	-	262530 ± 510	1.48 ± 0.01	-
TP22 VC026-22	170	-	-	258500 ± 510	1.71 ± 0.01	-
TP22 VC026-23	177	-	-	1062960 ± 1030	2.07 ± 0.01	-
TP22 VC026-24	184	-	-	944640 ± 970	2.03 ± 0.01	-
TP22 VC026-25	195	-	-	706500 ± 840	1.98 ± 0.01	-
TP22 VC026-26	201	-	-	723100 ± 850	2.03 ± 0.01	-
TP22 VC026-27	207	-	-	746990 ± 870	1.92 ± 0.01	-

Table S2: Distributions in apparent doses through cores TP22-VC03 (CERSA1202), TP22-VC07 (CERSA1200) and TP22-VC26 (CERSA1198)

Lab ID	Depth /cm	Apparent dose / Gy		Sensitivity / counts Gy^{-1}			Apparent dose / Gy	Sensitivity / counts Gy^{-1}
		Aliquot 1	Aliquot 2	Aliquot 1	Aliquot 2		mean	mean
CERSA1202/6	58	-	0.18 ± 0.10	220 ± 10	640 ± 30		0.18 ± 0.10	430 ± 210
CERSA1202/7	68	0.21 ± 0.13	0.05 ± 0.05	380 ± 20	960 ± 30		0.13 ± 0.08	670 ± 290
CERSA1202/8	78	2.94 ± 0.62	0.31 ± 0.04	160 ± 10	1870 ± 40		1.62 ± 1.31	1010 ± 850
CERSA1202/9	88	0.24 ± 0.04	0.18 ± 0.10	1250 ± 40	530 ± 20		0.21 ± 0.03	890 ± 360
CERSA1202/10	98	0.09 ± 0.07	1.09 ± 2.74	1140 ± 30	30 ± 10		0.59 ± 0.50	590 ± 560
CERSA1202/11	108	7.35 ± 1.40	1.07 ± 0.43	200 ± 10	130 ± 10		4.21 ± 3.14	170 ± 30
CERSA1202/12	118	0.35 ± 0.17	7.84 ± 0.46	310 ± 20	930 ± 30		4.10 ± 3.74	620 ± 310
CERSA1202/13	127	0.17 ± 0.30	0.50 ± 0.04	130 ± 10	1780 ± 40		0.34 ± 0.17	950 ± 830
CERSA1202/14	137	0.33 ± 0.03	0.41 ± 0.13	2170 ± 50	380 ± 20		0.37 ± 0.04	1270 ± 890
CERSA1202/15	141	0.84 ± 0.10	1.00 ± 0.23	560 ± 20	270 ± 20		0.92 ± 0.08	420 ± 140
CERSA1202/16	148	3.10 ± 0.16	19.83 ± 2.01	1430 ± 40	530 ± 20		11.46 ± 8.36	980 ± 450
CERSA1202/17	154	3.01 ± 0.12	4.54 ± 0.19	3190 ± 60	2190 ± 50		3.78 ± 0.76	2690 ± 500
CERSA1202/18	162	27.84 ± 1.94	4.30 ± 0.43	1000 ± 30	420 ± 20		16.07 ± 11.77	710 ± 290
CERSA1202/19	170	10.04 ± 0.24	89.15±11.99	15290 ± 120	5190 ± 70		49.6 ± 39.56	10240 ± 5050
CERSA1202/20	177	34.39 ± 1.45	59.29 ± 2.65	9890 ± 100	6330 ± 80		46.84 ± 12.45	8110 ± 1780
CERSA1202/21	187.5	54.93 ± 6.04	50.12 ± 2.92	1630 ± 40	4350 ± 70		52.53 ± 2.41	2990 ± 1360
CERSA1202/22	194.5	247.0±260.8	128.5 ±25.8	2240 ± 50	890 ± 30		187.7 ± 59.3	1560 ± 670
CERSA1202/23	200.5	57.59 ± 5.69	104.5 ± 13.4	1420 ± 40	820 ± 30		81.03 ± 23.44	1120 ± 300
CERSA1202/24	208.5	31.38 ± 1.25	77.31 ± 8.06	10920 ± 100	1780 ± 40		54.35 ± 22.97	6350 ± 4570

CERSA1202/25	217.5	59.5 ± 2.99	66.53 ± 3.66	14160 ± 120	9890 ± 100		63.02 ± 3.51	12020 ± 2140
CERSA1202/26	224.5	43.26 ± 3.32	98.07 ± 6.72	5470 ± 70	10680 ± 100		70.66 ± 27.4	8080 ± 2600
CERSA1202/27	232.5	43.09 ± 4.06	70.35±12.66	1000 ± 30	400 ± 20		56.72 ± 13.63	700 ± 300
CERSA1200/5	43.5	-	-	-	-		-	-
CERSA1200/6	52.5	0.40 ± 0.03	0.65 ± 0.08	3520 ± 60	1580 ± 40		0.52 ± 0.12	2550 ± 970
CERSA1200/7	63.5	0.84 ± 0.14	0.56 ± 0.08	510 ± 20	670 ± 30		0.70 ± 0.14	590 ± 80
CERSA1200/8	73.5	0.04 ± 0.26	0.68 ± 0.08	270 ± 20	940 ± 30		0.36 ± 0.32	610 ± 330
CERSA1200/9	83.5	0.43 ± 0.23	0.54 ± 0.17	190 ± 10	400 ± 20		0.48 ± 0.06	290 ± 110
CERSA1200/10	93.5	0.32 ± 0.14	0.76 ± 0.04	430 ± 20	2690 ± 50		0.54 ± 0.22	1560 ± 1130
CERSA1200/11	103.5	0.80 ± 0.21	0.86 ± 0.03	280 ± 20	8480 ± 90		0.83 ± 0.03	4380 ± 4100
CERSA1200/12	112.5	0.68 ± 0.10	0.62 ± 0.09	690 ± 30	920 ± 30		0.65 ± 0.03	800 ± 110
CERSA1200/13	116.5	1.28 ± 0.05	0.89 ± 0.04	2570 ± 50	3280 ± 60		1.08 ± 0.2	2930 ± 360
CERSA1200/14	125	0.75 ± 0.07	1.01 ± 0.28	1130 ± 30	270 ± 20		0.88 ± 0.13	700 ± 430
CERSA1200/15	134	0.62 ± 0.15	0.42 ± 0.13	280 ± 20	380 ± 20		0.52 ± 0.1	330 ± 50
CERSA1200/16	144	0.96 ± 0.05	0.66 ± 0.03	2920 ± 50	2430 ± 50		0.81 ± 0.15	2670 ± 240
CERSA1200/17	154	0.72 ± 0.04	0.72 ± 0.06	2950 ± 50	890 ± 30		0.72 ± 0	1920 ± 1030
CERSA1200/18	164	0.88 ± 0.05	0.70 ± 0.04	1480 ± 40	2190 ± 50		0.79 ± 0.09	1830 ± 360
CERSA1200/19	174	0.69 ± 0.04	0.65 ± 0.15	2470 ± 50	390 ± 20		0.67 ± 0.02	1430 ± 1040
CERSA1200/20	184	0.82 ± 0.15	0.79 ± 0.10	350 ± 20	560 ± 20		0.8 ± 0.02	450 ± 100
CERSA1200/21	194	0.84 ± 0.03	0.61 ± 0.04	6930 ± 80	2430 ± 50		0.72 ± 0.11	4680 ± 2250
CERSA1200/22	204	0.84 ± 0.07	0.51 ± 0.09	1370 ± 40	570 ± 20		0.67 ± 0.16	970 ± 400
CERSA1200/23	209	1.05 ± 0.10	1.55 ± 0.07	1360 ± 40	6210 ± 80		1.3 ± 0.25	3790 ± 2430
CERSA1198/4	35.5	0.75 ± 0.07	0.85 ± 0.2	800 ± 30	210 ± 10		0.80 ± 0.05	510 ± 300
CERSA1198/5	42.5	0.50 ± 0.05	0.90 ± 0.11	960 ± 30	750 ± 30		0.70 ± 0.20	850 ± 100
CERSA1198/6	50.5	0.83 ± 0.03	0.84 ± 0.10	20230 ± 140	560 ± 20		0.84 ± 0.01	10390 ± 9830
CERSA1198/7	56.5	0.91 ± 0.06	0.81 ± 0.03	2500 ± 50	3730 ± 60		0.86 ± 0.05	3120 ± 620
CERSA1198/8	61.5	1.10 ± 0.23	0.96 ± 0.13	210 ± 10	530 ± 20		1.03 ± 0.07	370 ± 160
CERSA1198/9	70.5	0.98 ± 0.08	1.15 ± 0.05	1380 ± 40	5340 ± 70		1.07 ± 0.08	3360 ± 1980
CERSA1198/10	80.5	1.02 ± 0.07	1.21 ± 0.26	1810 ± 40	150 ± 10		1.11 ± 0.1	980 ± 830
CERSA1198/11	90.5	0.89 ± 0.03	0.83 ± 0.04	4890 ± 70	5080 ± 70		0.86 ± 0.03	4990 ± 100
CERSA1198/12	100.5	0.87 ± 0.07	0.96 ± 0.05	1260 ± 40	2340 ± 50		0.92 ± 0.05	1800 ± 540
CERSA1198/13	110.5	0.70 ± 0.07	1.32 ± 0.26	1080 ± 30	160 ± 10		1.01 ± 0.31	620 ± 460
CERSA1198/14	117.5	11.06 ± 1.93	0.78 ± 0.05	430 ± 20	1950 ± 40		5.92 ± 5.14	1190 ± 760
CERSA1198/15	123	1.17 ± 0.55	2.73 ± 1.18	120 ± 10	70 ± 10		1.95 ± 0.78	100 ± 20
CERSA1198/16	129	1.02 ± 0.11	0.98 ± 0.41	580 ± 20	150 ± 10		1 ± 0.02	360 ± 220
CERSA1198/17	133	0.89 ± 0.09	0.61 ± 0.02	650 ± 30	14760 ± 120		0.75 ± 0.14	7710 ± 7060
CERSA1198/18	139	0.82 ± 0.61	0.85 ± 0.14	60 ± 10	370 ± 20		0.84 ± 0.02	220 ± 150
CERSA1198/19	150	0.40 ± 0.09	1.02 ± 0.13	550 ± 20	460 ± 20		0.71 ± 0.31	500 ± 40
CERSA1198/20	158	0.62 ± 0.04	0.7 ± 0.08	1820 ± 40	950 ± 30		0.66 ± 0.04	1390 ± 440
CERSA1198/21	166	0.73 ± 0.11	0.98 ± 0.23	450 ± 20	230 ± 20		0.85 ± 0.13	340 ± 110
CERSA1198/22	170	5.10 ± 1.68	2.73 ± 0.4	110 ± 10	250 ± 20		3.91 ± 1.19	180 ± 70
CERSA1198/23	177	7.37 ± 1.00	5.20 ± 0.52	480 ± 20	500 ± 20		6.28 ± 1.08	490 ± 10
CERSA1198/24	184	3.94 ± 0.50	5.10 ± 0.25	410 ± 20	1340 ± 40		4.52 ± 0.58	870 ± 470
CERSA1198/25	195	8.53 ± 1.06	7.86 ± 1.54	1400 ± 40	170 ± 10		8.19 ± 0.33	780 ± 620
CERSA1198/26	201	4.26 ± 0.38	6.08 ± 0.97	840 ± 30	920 ± 30		5.17 ± 0.91	880 ± 40
CERSA1198/27	207	4.73 ± 0.57	4.24 ± 0.48	330 ± 20	920 ± 30		4.49 ± 0.25	630 ± 300

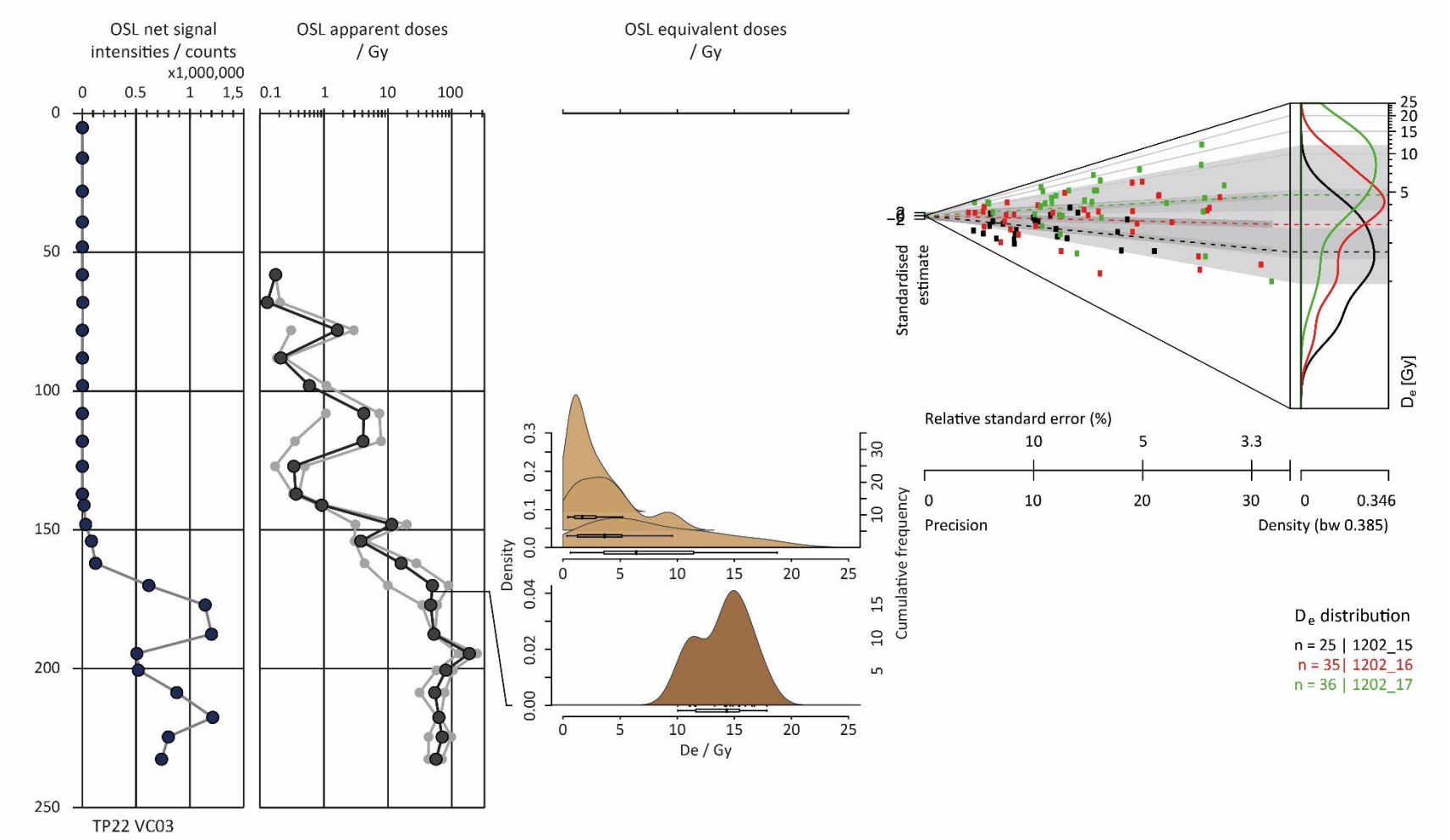

Figure S1: TP22-VC03 (CERSA1202 and 1203)

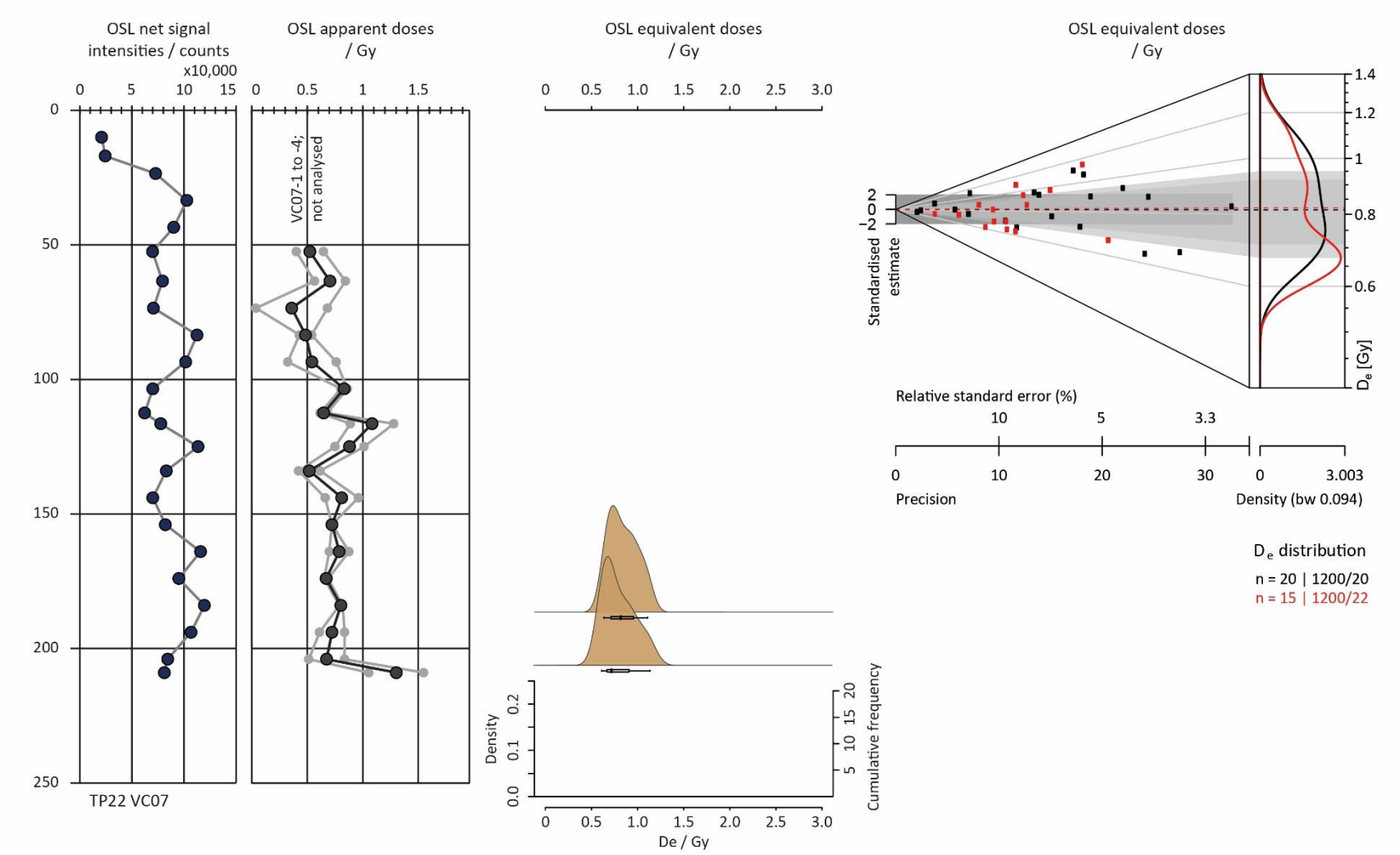

Figure S2: TP22-VC07 (CERSA1200 and 1201)

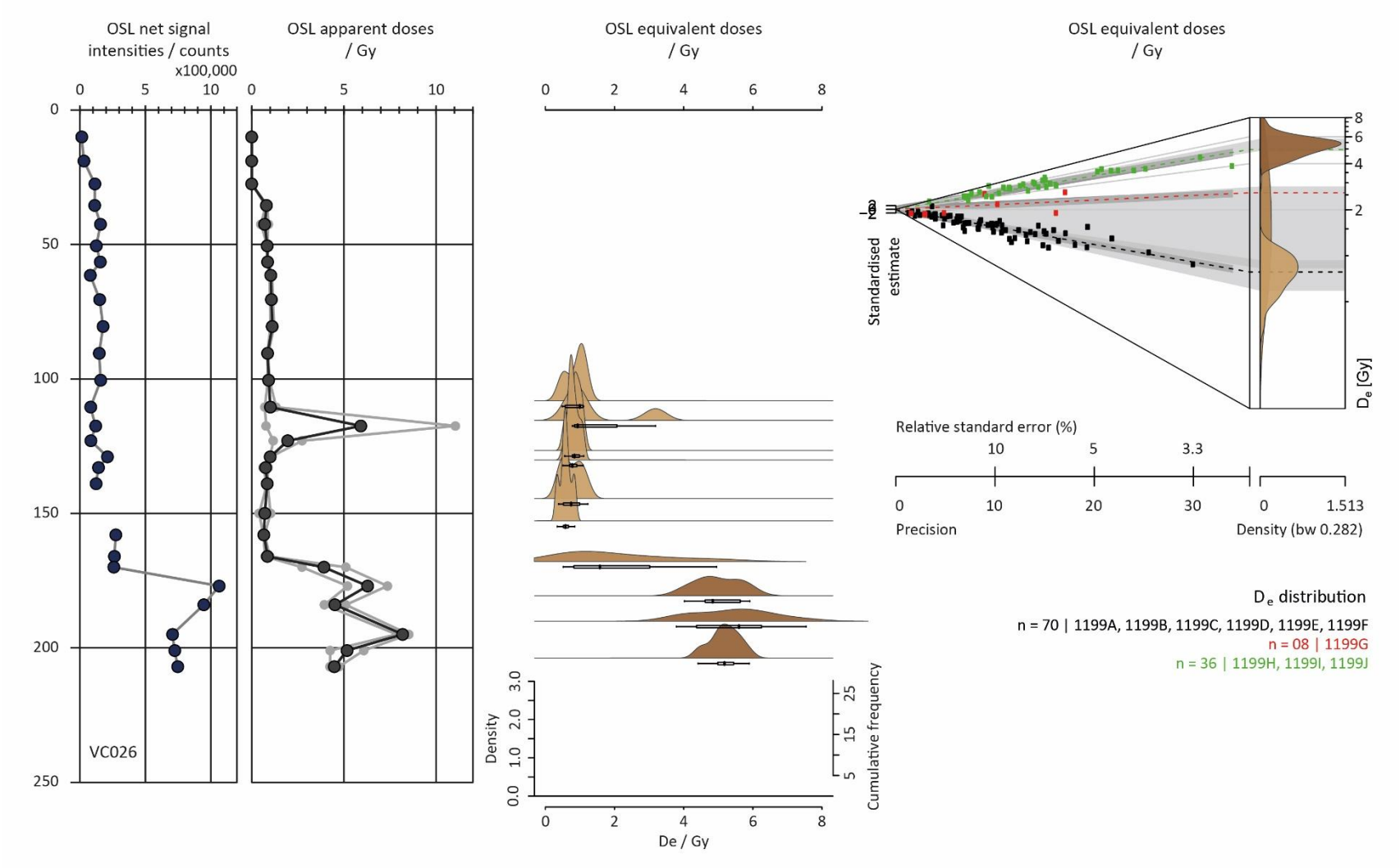

Figure S3: TP22-VC26 (CERSA1998 and 1999)

Stage 3: Quartz SAR OSL dating

A luminescence age is the quotient of the burial dose (in Gy) over the effective environmental dose rate (in mGy a^{-1}). Here, equivalent dose (De) determinations – used to estimate the burial dose - were made on sets of ~24 aliquots using the single aliquot regenerative dose (SAR) OSL protocol. The dose rates to these sediments were assessed using the combination of low-level radioactivity measurements in the laboratory, and determinations of radionuclide concentrations by mass spectrometry.

Equivalent dose determinations. Mineral separation procedures similar to those used by (Kinnaird et al., 2017) were used to extract HF-etched 'quartz' from all samples. Samples were wet sieved to obtain the 90 to 250 µm fractions. These fractions were then treated in 1M HCl for 10 minutes, 40% HF for 40 minutes, and a further 1M HCl for 10 minutes. The 90 to 250 µm, HF-etched fractions were density separated in LST fast float solutions of 2.64 and 2.74 gcm^{-3}. The 90-250 µm, HF-etched, 2.64-2.74 gcm^{-3} fractions were re-sieved at 150 µm, and the 150-250 µm fractions dispensed to 10mm stainless steel discs for measurement. OSL measurements were carried out using a Risø TL/OSL DA-20 automated dating system.

Data reduction and De determinations were made in Luminescence Analyst v.4.31.9 and the package Luminescence in R. Individual decay curves were scrutinised for shape and consistency. Dose response curves were fitted with an exponential function, with the growth curve fitted through zero and the repeat recycling points. Error analysis was determined by Monte Carlo Stimulation.

Aliquots satisfying the following criteria were accepted for assimilation of Des: 1) recuperation of less than 5 %; 2) recycling ratio within 10 % of unity, including uncertainties (Murray and Wintle, 2003); 3) OSL IR depletion ratio within 10 % of unity (Duller, 2003) and 4) test dose signals 3σ greater than background levels.

Equivalent dose distributions. The equivalent dose distributions for the samples taken forward to dating from cores TP22-VC03, TP22-VC07 and TP22-VC26 are shown as kernel density estimate (KDE) and Abanico plots in figures S1 to S3. The complexity to these distributions varies by core and, by position in the sequence:

- TP22-VC03: sampling the oldest part of the sand body: samples CERSA1202-15, -16 and -17 show the greatest complexity, with distributions ranging from the sub-Gy to in excess of 5 Gy and overdispersions > 50%;
- TP22-VC07: sampling the most recent erosional event / youngest part of the sand body: samples CERSA1200-20 and -22 have tighter distributions, ranging between 0.6 and 1.1 Gy and overdispersions in the range 16-18%;
- TP22-VC26: samples CERSA1998-A to J show a range of distributions, from tight to broad with overdispersions ~9 to 60 %.

For age assimilation below, the **weighted mean** and standard deviation of the distribution were used in determining depositional ages.

Radionuclide concentrations and Environmental dose rates. Radionuclide concentrations of ^{232}Th, ^{238}U and ^{40}K were determined from inductively coupled plasma mass spectrometry (ICP-MS; U, Th) and inductively coupled plasma optical emission spectrometry (ICP-OES; K) at Chemostrat's Welshpool Laboratory (Table S3). Infinite matrix dose rates were calculated from these using the conversion factors of Guérin et al. (2011) and adjusted for attenuation by grain size and chemical etching using the datasets of Guérin et al. (2012) and Bell (1979) respectively (Table S4).

Activity concentrations of ^{232}Th, ^{238}U and ^{40}K, and estimates of beta and gamma dose rate, were also obtained from environmental radioactivity measurements using a MiDose Solutions µDose unit (S/N 016: Tudyka et al., 2018; Kolb et al., 2022) (Table S5). These estimates of beta and gamma dose rate were combined using weighted statistics with the infinite matrix dose rates obtained from ICP-MS and ICP-OES.

Water contents were determined for all samples in the laboratory, with values of values of c. 15–25% adopted to determine effective environmental dose rates (Ḋ). The dose rates measurements were used in combination with the assumed burial water contents to determine the total effective dose rates for age estimation (Table S6).

The contributions from the cosmic dose were modelled after (Sanderson and Kinnaird, 2019), by combining latitude and altitude specific dose rates (0.19 ± 0.07 mGy a^{-1}), with time-dependent corrections for water depth and overburden as follows, based on the following assumptions:

- TP22-VC03 and TP22-VC07: the sands forming the Stroombank were deposited offshore (bleached during transport) and almost instantaneously flooded. Current depth of water 11.1 m and 12.0 m, respectively.
- TP22-VC26: the sands forming the Stroombank deposited offshore (bleached during transport) and almost instantaneously flooded; the coarse-sands / gravels at the base of the Stroombank were deposited in an offshore to near-shore environment and the underlying sands, in a near-shore to shoreline setting. The sands underneath the Stroombank might have received a contribution from the cosmic dose between deposition and inundation sometime between 500BC and 500AD.

Table S3: ICP-MS and ICP-OES determinations of K (%), U and Th (ppm) concentrations

Core	*Lab code / CERSA#*	*Depth in core /cm*	K / %	U / ppm	Th / ppm
TP22-VC26	1199A	105.5-110.5	1.18 ± 0.06	0.58 ± 0.03	1.71 ± 0.09
	1199B	100.5-115.5	0.82 ± 0.04	0.59 ± 0.03	1.75 ± 0.09
	1199C	124-129	0.76 ± 0.04	0.54 ± 0.03	1.5 0± 0.08
	1199D	130-133	0.73 ± 0.04	0.56 ± 0.03	1.37 ± 0.07
	1199E	140-145	0.49 ± 0.02	0.55 ± 0.03	1.14 ± 0.06
	1199F	151-155	0.45 ± 0.02	0.56 ± 0.03	1.11 ± 0.06
	1199G	166-170	0.36 ± 0.02	0.51 ± 0.03	0.85 ± 0.04
	1199H	177-183	0.98 ± 0.05	0.56 ± 0.03	1.83 ± 0.09
	1199I	185-190	1.07 ± 0.05	0.62 ± 0.03	2.16 ± 0.11
	1199J	202-205	1.04 ± 0.05	0.78 ± 0.04	2.05 ± 0.10
TP22-VC07	1201A	33.5-38.5	0.79 ± 0.04	0.78 ± 0.04	1.68 ± 0.08
	1201D	189-194	0.84 ± 0.04	0.47 ± 0.02	1.58 ± 0.08
	1201E	199-204	0.79 ± 0.04	0.47 ± 0.02	1.38 ± 0.07
TP22-VC03	1203A	155-160	0.78 ± 0.04	0.72 ± 0.04	2.42 ± 0.12
	1203B	162-166	0.65 ± 0.03	0.49 ± 0.02	1.44 ± 0.07
	1203C	171-175	0.82 ± 0.04	0.51 ± 0.03	1.75 ± 0.09

Table S4: Infinite matrix dose rates determined from ICP-MS and ICP-OES and alpha- and beta-counting

Core	*Lab code/ CERSA#*	ICP-MS and ICP-OES			α and β counts, uDose		
		Alpha, dry / mGy a^{-1}	Beta, dry / mGy a^{-1}	Gamma, dry / mGy a^{-1}	Alpha, dry / mGy a^{-1}	Beta, dry / mGy a^{-1}	Gamma, dry / mGy a^{-1}
TP22-VC26	1199A	2.87 ± 0.10	1.02 ± 0.05	0.44 ± 0.02	2.71 ± 0.14	1.01 ± 0.06	0.40 ± 0.02
	1199B	2.95 ± 0.11	0.75 ± 0.03	0.36 ± 0.01	2.58 ± 0.12	0.66 ± 0.05	0.30 ± 0.02
	1199C	2.63 ± 0.09	0.68 ± 0.03	0.32 ± 0.01	2.49 ± 0.13	0.64 ± 0.05	0.29 ± 0.02
	1199D	2.58 ± 0.09	0.66 ± 0.03	0.31 ± 0.01	3.54 ± 0.27	0.85 ± 0.06	0.44 ± 0.03
	1199E	2.38 ± 0.09	0.47 ± 0.02	0.24 ± 0.01	2.09 ± 0.10	0.41 ± 0.04	0.18 ± 0.01
	1199F	2.37 ± 0.09	0.44 ± 0.02	0.23 ± 0.01	1.76 ± 0.12	0.29 ± 0.04	0.18 ± 0.02
	1199G	2.05 ± 0.08	0.36 ± 0.01	0.19 ± 0.01	0.25 ± 0.03	0.23 ± 0.04	0.18 ± 0.02
	1199H	2.92 ± 0.10	0.86 ± 0.04	0.39 ± 0.01	0.43 ± 0.05	0.63 ± 0.05	0.35 ± 0.03
	1199I	3.32 ± 0.12	0.95 ± 0.04	0.44 ± 0.01	0.31 ± 0.03	0.59 ± 0.05	0.33 ± 0.02
	1199J	3.68 ± 0.13	0.94 ± 0.04	0.44 ± 0.01	0.34 ± 0.04	0.62 ± 0.05	0.28 ± 0.02
VC07	1201A	3.41 ± 0.12	0.74 ± 0.03	0.36 ± 0.01	-	-	-
	1201C	-	-	-	0.20 ± 0.02	0.16 ± 0.04	0.11 ± 0.01
	1201D	2.48 ± 0.09	0.74 ± 0.03	0.34 ± 0.01	0.23 ± 0.03	0.19 ± 0.04	0.15 ± 0.02
	1201E	2.32 ± 0.08	0.70 ± 0.03	0.31 ± 0.01	0.19 ± 0.02	0.15 ± 0.04	0.13 ± 0.02
TP22-VC03	1203A	3.78 ± 0.13	0.75 ± 0.03	0.39 ± 0.01	0.32 ± 0.03	0.54 ± 0.05	0.30 ± 0.03
	1203B	2.45 ± 0.09	0.60 ± 0.03	0.29 ± 0.01	0.22 ± 0.04	0.22 ± 0.04	0.20 ± 0.02
	1203C	2.71 ± 0.10	0.73 ± 0.03	0.34 ± 0.01	0.24 ± 0.03	0.21 ± 0.04	0.13 ± 0.02

Table S5a: Total environmnetal dose rates: [a]Effective beta dose rate combining water content corrections with inverse grain size attenuation factors obtained Mejdahl (1979) for K, U, and Th; [b] gamma dose rates reconciled using a distance-weigthed contribution; [c]includes a cosmic dose contribution, modelled assuming inudation at AD 500; [d,e,f] derived from [d] ICP-OES, ICP-MS, alpha and beta counting, [e] alpha and beta counting, and [f] ICP-OES and ICP-MS, weighted by error

Core	*Lab code / CERSA#*	Water content / %	Cosmic dose / mGy a^{-1}	Effective dose rates, wet / mGy a^{-1}		
				Beta [a]	Gamma [b]	Total [c]
TP22-VC26	1199A [d]	22 ± 7	0.06 ± 0.01	0.81 ± 0.05	0.29 ± 0.04	1.16 ± 0.06
	1199B [d]	20 ± 6	0.06 ± 0.01	0.58 ± 0.03	0.28 ± 0.04	0.91 ± 0.05
	1199C [d]	19 ± 6	0.06 ± 0.01	0.55 ± 0.03	0.25 ± 0.03	0.85 ± 0.05
	1199D [d]	20 ± 6	0.06 ± 0.01	0.58 ± 0.03	0.24 ± 0.03	0.88 ± 0.05
	1199E [d]	19 ± 6	0.05 ± 0.01	0.37 ± 0.02	0.20 ± 0.04	0.62 ± 0.04
	1199F [d]	18 ± 5	0.05 ± 0.01	0.33 ± 0.02	0.18 ± 0.04	0.56 ± 0.04
	1199G [d]	18 ± 5	0.05 ± 0.01	0.27 ± 0.02	0.18 ± 0.04	0.51 ± 0.04
	1199H [d]	21 ± 6	0.12 ± 0.02	0.59 ± 0.04	0.25 ± 0.04	0.96 ± 0.06
	1199I [d]	20 ± 6	0.12 ± 0.02	0.59 ± 0.04	0.28 ± 0.04	0.98 ± 0.06
	1199J [d]	23 ± 7	0.11 ± 0.02	0.60 ± 0.04	0.27 ± 0.05	0.99 ± 0.06
TP22-VC07	1201A [e]	17 ± 5	0.06 ± 0.01	0.63 ± 0.04	0.31 ± 0.06	0.93 ± 0.07
	1201C [f]	18 ± 5	0.05 ± 0.01	0.16 ± 0.04	0.11 ± 0.09	0.27 ± 0.10
	1201D [d]	22 ± 7	0.05 ± 0.01	0.35 ± 0.03	0.20 ± 0.01	0.60 ± 0.03
	1201E [d]	22 ± 7	0.05 ± 0.01	0.33 ± 0.03	0.19 ± 0.01	0.56 ± 0.03
TP22-VC03	1203A [d]	20 ± 6	0.05 ± 0.01	0.58 ± 0.03	0.26 ± 0.04	0.89 ± 0.05
	1203B [d]	19 ± 6	0.05 ± 0.01	0.36 ± 0.03	0.24 ± 0.04	0.64 ± 0.05
	1203C [d]	22 ± 7	0.05 ± 0.01	0.37 ± 0.03	0.21 ± 0.05	0.62 ± 0.05

Table S5b: Total environmnetal dose rates. [a]Effective beta dose rate combining water content corrections with inverse grain size attenuation factors obtained Mejdahl (1979) for K, U, and Th; [b] gamma dose rates reconciled using a distance-weigthed contribution; [c]includes a cosmic dose contribution, modelled assuming inudation at 500 BC; [d] derived from ICP-OES, ICP-MS, alpha and beta counting

Lab code / CERSA#	Water content / %	Cosmic dose / mGy a^{-1}	Effective dose rates, wet / mGy a^{-1}		
			Beta [a]	Gamma [b]	Total [c]
1199H [d]	21 ± 6	0.10 ± 0.02	0.59 ± 0.04	0.25 ± 0.04	0.95 ± 0.06
1199I [d]	20 ± 6	0.10 ± 0.02	0.59 ± 0.04	0.28 ± 0.04	0.97 ± 0.06
1199J [d]	23 ± 7	0.10 ± 0.02	0.60 ± 0.04	0.27 ± 0.05	0.97 ± 0.06

Age Assimilation. Table S6 lists the burial doses, the total effective dose rates and the corresponding depositional ages for TP22-VC03, TP22-VC07 and TP22-VC26.

TP22-VC26 (CERSA1998/1999): the consistency between the stage 1 and stage 2 datasets, and the spatial associations between the dating positions down core, mean that several weighted combinations can be considered:

- for the lower part of the sequence, the weighted combination of CERSA1199H, 1199I and 1199J, assuming inundation by 500 CE, is 5.03 ± 0.24 (3010 ± 240 BCE); or assuming earlier inundation around 500 CE, 5.13 ± 0.25 (3110 ± 250 BCE)
- the gravels were deposited at ~ 1.05 ± 0.10 ka (980 ± 100 CE)
- and the sand body no later than 0.89 ± 0.05 ka (1130 ± 50 CE)

TP22-VC07 (CERSA1200/1201): the Stroombank – as recovered in core TP22-VC07 – is dated to 780 ± 120 CE (CERSA1200/20) to 720 ± 170 CE (CERSA1200/22), or 760 ± 100 CE, the weighted combination of the two.

TP22-VC03 (CERSA1202/1203): the sands beneath the erosional surface are characterised by the broad equivalent dose distributions, reflecting mixing of a well-bleached component and sediment carrying luminescence residuals. The dates for these sands are poorly resolved, suggesting deposition in the late first millennium, 930 ± 290 CE and 930 ± 540 CE (CERSA1202/15 and CERSA1202/16, respectively). The weighted combination of these two depositional ages is 940 ± 250 CE.

Table S6: Burial doses, total effective environmnetal dose rates and corresponding depositional ages for VC02, VC07 and TP22-VC26 (CERSA1202, 1200 and 1198); [4a] assuming inudation by 500 CE, [4b] by 500 BC.

Core	Depth (cm)	CERSA #	Burial dose /Gy	Total effective dose rate / mGy a^{-1}	Age / ka	Calendar years
TP22-VC26	105.5-110.5	1199A	0.97 ± 0.19	1.16 ± 0.06	0.83 ± 0.17	1190 ± 170 CE
	110.5-115.5	1199B	0.90 ± 0.11	0.91 ± 0.05	0.98 ± 0.13	1040 ± 130 CE
	124-129	1199C	0.74 ± 0.07	0.85 ± 0.05	0.87 ± 0.10	1150 ± 100 CE
	130-133	1199D	0.78 ± 0.04	0.88 ± 0.05	0.89 ± 0.06	1130 ± 60 CE
	140-145	1199E	0.62 ± 0.11	0.62 ± 0.04	1.00 ± 0.19	1020 ± 190 CE
	151-155	1199F	0.60 ± 0.05	0.56 ± 0.04	1.07 ± 0.12	950 ± 120 CE
	166-170	1199G	1.90 ± 0.56	0.51 ± 0.04	3.75 ± 1.16	1730 ± 1160 BCE
	177-183	1199H	4.92 ± 0.21	0.96 ± 0.06 [4a] 0.95 ± 0.06 [4b]	5.11 ± 0.37 [4a] 5.21 ± 0.38 [4b]	3090 ± 370 BCE [4a] 3190 ± 380 BCE [4a]
	185-190	1199I	4.54 ± 0.59	0.98 ± 0.06 [4a] 0.97 ± 0.06 [4b]	4.61 ± 0.65 [4a] 4.70 ± 0.67 [4b]	2590 ± 650 BCE [4a] 2680 ± 670 BCE [4b]
	202-205	1199J	5.03 ± 0.14	0.99 ± 0.06 [4a] 0.97 ± 0.06 [4b]	5.09 ± 0.36 [4a] 5.19 ± 0.37 [4b]	3070 ± 360 BCE [4a] 3170 ± 370 BCE [4b]

TP22-VC07	184	1200-20	0.78 ± 0.05	0.63 ± 0.05	1.24 ± 0.12	780 ± 120 CE
	204	1200-22	0.72 ± 0.08	0.56 ± 0.04	1.30 ± 0.17	720 ± 170 CE
TP22-VC03	141	1202-15	0.97 ± 0.21	0.89 ± 0.14	1.09 ± 0.29	930 ± 290 CE
	148	1202-16	0.96 ± 0.46	0.89 ± 0.14	1.08 ± 0.54	940 ± 540 CE
	154	1202-17	1.36 ± 0.97	0.89 ± 0.05	1.54 ± 1.10	~ 1st millennium CE
	170	1202-19	51.54 ±2.92	0.62 ± 0.05	83.13 ± 8.20	

References

Bell, W.T., 1979. Attenuation factors for the absorbed radiation dose in quartz inclusions for thermoluminescence dating. Anc. TL 8, 1–12. https://doi.org/10.26034/la.atl.1979.022

Duller, G.A.T., 2003. Distinguishing quartz and feldspar in single grain luminescence measurements. Radiat. Meas. 37, 161–165. https://doi.org/10.1016/S1350-4487(02)00170-1

Guérin, G., Mercier, N., Adamiec, G., 2011. Dose-rate conversion factors: update. Anc. TL 29, 5–8. https://doi.org/10.26034/la.atl.2011.443

Guérin, G., Mercier, N., Nathan, R., Adamiec, G., Lefrais, Y., 2012. On the use of the infinite matrix assumption and associated concepts: a critical review. Radiat. Meas. 47, 778–785. https://doi.org/10.1016/j.radmeas.2012.04.004

Kinnaird, T., Bolòs, J., Turner, A., Turner, S., 2017. Optically-stimulated luminescence profiling and dating of historic agricultural terraces in Catalonia (Spain). J. Archaeol. Sci. 78, 66–77. https://doi.org/10.1016/j.jas.2016.11.003

Kolb, T., Tudyka, K., Kadereit, A., Lomax, J., Poręba, G., Zander, A., Zipf, L., Fuchs, M., 2022. The µDose system: determination of environmental dose rates by combined alpha and beta counting – performance tests and practical experiences. Geochronology 4, 1–31. https://doi.org/10.5194/gchron-4-1-2022

Lichtenberger, A., Raja, R., Seland, E.H., Kinnaird, T., Simpson, I.A., 2019. Urban-riverine hinterland synergies in semi-arid environments: millennial-scale change, adaptations, and environmental responses at Gerasa/Jerash. J. Field Archaeol. 44, 333–351. https://doi.org/10.1080/00934690.2019.1625619

Mejdahl, V., 1979. Thermoluminescence dating: beta-dose attenuation in quartz grains. Archaeometry 21, 61–72. https://doi.org/10.1111/j.1475-4754.1979.tb00241.x

Munyikwa, K., Kinnaird, T.C., Sanderson, D.C.W., 2021. The potential of portable luminescence readers in geomorphological investigations: a review. Earth Surf. Process. Landf. 46, 131–150. https://doi.org/10.1002/esp.4975

Murray, A.S., Wintle, A.G., 2003. The single aliquot regenerative dose protocol: potential for improvements in reliability. Radiat. Meas. 37, 377–381. https://doi.org/10.1016/S1350-4487(03)00053-2

Sanderson, D.C.W., Kinnaird, T.C., 2019. Optically stimulated luminescence dating as a geochronological tool for late Quaternary sediments in the Red Sea region, in: Rasul, N.M.A., Stewart, I.C.F. (Eds.), Geological Setting, Palaeoenvironment and Archaeology of the Red Sea. Springer International Publishing, Cham, pp. 685–707. https://doi.org/10.1007/978-3-319-99408-6_31

Tudyka, K., Miłosz, S., Adamiec, G., Bluszcz, A., Poręba, G., Paszkowski, Ł., Kolarczyk, A., 2018. µDose: a compact system for environmental radioactivity and dose rate measurement. Radiat. Meas. 118, 8–13. https://doi.org/10.1016/j.radmeas.2018.07.016

Turner, S., Kinnaird, T., Varinlioğlu, G., Şerifoğlu, T.E., Koparal, E., Demirciler, V., Athanasoulis, D., Ødegård, K., Crow, J., Jackson, M., Bolòs, J., Sánchez-Pardo, J.C., Carrer, F., Sanderson, D., Turner, A., 2021. Agricultural terraces in the Mediterranean: medieval intensification revealed by OSL profiling and dating. Antiquity 95, 773–790. https://doi.org/10.15184/aqy.2020.187

Vervust, S., Kinnaird, T., Herring, P., Turner, S., 2020. Optically stimulated luminescence profiling and dating of earthworks: the creation and development of prehistoric field boundaries at Bosigran, Cornwall. Antiquity 94, 420–436. https://doi.org/10.15184/aqy.2019.138

Report. Optically stimulated luminescence profiling and dating of cores TP22-VC04, TP22-VC05, TP22-VC06-1, TP22-VC24, TP22-VC25, TP22-VC38 and TP23-VC43

Tim Kinnaird, Aayush Srivastava
School of Earth and Environmental Sciences, University of St Andrews

Soetkin Vervust
Archaeology, Environmental Changes, and Geo-Chemistry (AMGC), Vrije Universiteit Brussel

Víctor Cartelle, Ruth Plets
Flanders Marine Institute (VLIZ)

Introduction

This supplementary data file concerns the optically stimulated luminescence investigations of cores TP22-VC04, TP22-VC05, TP22-VC06-1, TP22-VC24, TP22-VC25, TP22-VC38 and TP23-VC43, together with new profiling of core TP22-VC26.

Sampling and OSL screening

Sampling was undertaken by Soetkin Vervust and Víctor Cartelle between the 2nd and 3rd of May 2024. Table S7 lists the IRSL and OSL net signal intensities, IRSL and OSL depletion indices and IRSL:OSL ratios observed through TP22-VC04, TP22-VC05, TP22-VC06-1, TP22-VC24, TP22-VC25, TP22-VC26, TP23-VC43 and TP22-VC38. It is important to note that these measurements were made on the VUB portable OSL instrument, and that the photomultiplier in this unit has different characteristics and sensitivity to the photomultiplier in the St. Andrews instrument, as used for TP22-VC03, TP22-VC07 and TP22-VC26: signal-depth progressions and breaks should be comparable, the magnitude in signal intensities will not. Therefore, new profiling was performed for core TP22-VC26.

Table S7: IRSL and OSL signal intensities and IRSL and OSL depletion indices for TP22-VC04, TP22-VC05, TP22-VC06-1, TP22-VC24, TP22-VC25, TP22-VC26, TP22-VC43 and TP22-VC38.

Core	Depth / cm	IRSL signal intensities / counts	IRSL depletion	OSL signal intensities / counts	OSL depletion
TP22-VC04	20	2630 ± 60	1.36 ± 0.06	18080 ± 140	1.6 ± 0.02
	45	4140 ± 70	1.42 ± 0.05	27800 ± 170	1.73 ± 0.02
	60	6790 ± 90	1.39 ± 0.04	39030 ± 200	1.74 ± 0.02
	80	4670 ± 80	1.4 ± 0.04	37930 ± 200	1.85 ± 0.02
	100	3760 ± 70	1.36 ± 0.05	24960 ± 160	1.66 ± 0.02
	120	3890 ± 70	1.39 ± 0.05	27350 ± 170	1.79 ± 0.02
	145	3520 ± 70	1.39 ± 0.05	25040 ± 160	1.74 ± 0.02
	160	3650 ± 70	1.38 ± 0.05	21250 ± 150	1.72 ± 0.02
	180	4040 ± 70	1.4 ± 0.05	27030 ± 170	1.79 ± 0.02
	194	2470 ± 60	1.27 ± 0.06	19050 ± 140	1.55 ± 0.02
	207	4280 ± 70	1.41 ± 0.05	26070 ± 170	1.66 ± 0.02
	220	2540 ± 60	1.31 ± 0.06	16970 ± 130	1.69 ± 0.03
	227	4810 ± 80	1.33 ± 0.04	30910 ± 180	1.64 ± 0.02
TP22-VC05	40	2590 ± 60	1.16 ± 0.05	26870 ± 170	1.25 ± 0.02
	80	28340 ± 170	1.31 ± 0.02	165210 ± 410	1.81 ± 0.01
	120	20450 ± 150	1.27 ± 0.02	116870 ± 340	1.77 ± 0.01
	160	22610 ± 150	1.31 ± 0.02	125540 ± 360	1.8 ± 0.01
TP22-VC06-1	30	6630 ± 90	1.33 ± 0.03	50610 ± 230	1.57 ± 0.01
	50	44590 ± 210	1.31 ± 0.01	271130 ± 520	1.88 ± 0.01
	80	45850 ± 220	1.36 ± 0.01	250500 ± 500	1.82 ± 0.01

	110	32890 ± 180	1.34 ± 0.02	191390 ± 440	1.86 ± 0.01
	140	24910 ± 160	1.34 ± 0.02	185200 ± 430	1.81 ± 0.01
	155	438480 ± 670	1.29 ± 0	3577470 ± 1900	1.89 ± 0
	168	3124960 ± 1770	1.31 ± 0	16344390 ± 4050	1.81 ± 0
	180	3931940 ± 1990	1.27 ± 0	21282090 ± 4630	1.76 ± 0
TP22-VC24	30	530 ± 40	1.12 ± 0.11	12710 ± 120	1.18 ± 0.02
	60	1450 ± 50	1.22 ± 0.07	14020 ± 120	1.34 ± 0.02
	90	12890 ± 120	1.33 ± 0.02	112120 ± 340	1.97 ± 0.01
	110	6720 ± 90	1.26 ± 0.03	93600 ± 310	1.85 ± 0.01
	130	17240 ± 140	1.29 ± 0.02	118600 ± 350	1.77 ± 0.01
	150	47280 ± 220	1.29 ± 0.01	393500 ± 630	1.95 ± 0.01
	170	49110 ± 220	1.27 ± 0.01	368300 ± 610	1.81 ± 0.01
	190	16080 ± 130	1.31 ± 0.02	103910 ± 330	1.82 ± 0.01
	200	17470 ± 140	1.27 ± 0.02	133110 ± 370	1.83 ± 0.01
	206	41790 ± 210	1.32 ± 0.01	311440 ± 560	1.9 ± 0.01
TP22-VC25	30	920 ± 40	1.45 ± 0.1	11360 ± 110	1.35 ± 0.03
	60	11220 ± 110	1.29 ± 0.02	70570 ± 270	1.81 ± 0.01
	90	7800 ± 90	1.27 ± 0.03	41950 ± 210	1.65 ± 0.02
	140	9970 ± 100	1.28 ± 0.03	60220 ± 250	1.74 ± 0.01
	170	12440 ± 120	1.29 ± 0.02	68850 ± 260	1.75 ± 0.01
	200	9220 ± 100	1.34 ± 0.03	53360 ± 230	1.74 ± 0.02
TP22-VC26	31	13810 ± 120	1.33 ± 0.02	81670 ± 290	1.76 ± 0.01
	47	30340 ± 180	1.37 ± 0.02	176220 ± 420	1.82 ± 0.01
	75	23170 ± 160	1.36 ± 0.02	130980 ± 360	1.86 ± 0.01
	96	22400 ± 150	1.33 ± 0.02	138730 ± 380	1.73 ± 0.01
	113	26970 ± 170	1.38 ± 0.02	172020 ± 420	1.82 ± 0.01
	125	48440 ± 220	1.39 ± 0.01	316200 ± 570	1.67 ± 0.01
	131	24890 ± 160	1.31 ± 0.02	221250 ± 470	1.61 ± 0.01
	141	24040 ± 160	1.25 ± 0.02	283030 ± 540	1.31 ± 0
	168	35170 ± 190	1.21 ± 0.01	378050 ± 620	1.42 ± 0
	186	205270 ± 460	1.35 ± 0.01	1144170 ± 1070	1.97 ± 0
TP23-VC43	30	1040 ± 50	1.47 ± 0.1	5590 ± 80	1.56 ± 0.04
	90	1770 ± 50	1.2 ± 0.06	12680 ± 120	1.62 ± 0.03
	120	1970 ± 50	1.17 ± 0.06	13690 ± 120	1.49 ± 0.03
	133	4100 ± 70	1.24 ± 0.04	34220 ± 190	1.67 ± 0.02
	150	3390 ± 70	1.33 ± 0.05	24180 ± 160	1.7 ± 0.02
	166	101910 ± 320	1.25 ± 0.01	840950 ± 920	1.76 ± 0
	170	166520 ± 410	1.27 ± 0.01	1776840 ± 1340	2.03 ± 0
	180	3362270 ± 1840	1.35 ± 0	18257130 ± 4280	1.98 ± 0
	190	2486200 ± 1580	1.27 ± 0	17797870 ± 4230	1.85 ± 0
	210	2419710 ± 1560	1.25 ± 0	20203740 ± 4510	1.93 ± 0
	240	2021640 ± 1430	1.27 ± 0	14824510 ± 3860	1.84 ± 0
TP22-VC38	30	3270 ± 70	1.22 ± 0.05	24360 ± 160	1.1 ± 0.01
	60	3090 ± 60	1.37 ± 0.05	27050 ± 170	1.47 ± 0.02
	110	5050 ± 80	1.34 ± 0.04	42630 ± 210	1.46 ± 0.01
	140	7330 ± 90	1.33 ± 0.03	62390 ± 250	1.4 ± 0.01
	170	2880 ± 60	1.33 ± 0.05	32060 ± 180	1.45 ± 0.02

Table S8: Details of dated samples.

Core	CERSA#	Sub-sample	Depth / cm	Associated samples
VC04	1574	-	152	VC04-145 and VC04-160
VC05	1575	-	150	VC05-120 and VC05-160
VC06	1576	-	125	VC06-110 and VC06-140
VC06	1577	-	172	VC06-168 and VC06-180
VC24	1578	-	100	VC24-90 and VC24-110
VC24	1579	-	158	VC24-150 and VC24-170
VC25	1580	-	185	VC25-170 and VC25-200

Quartz SAR OSL dating

A luminescence age is the quotient of the burial dose (in Gy) over the effective environmental dose rate (in mGy a^{-1}). It requires that the sediment was fully bleached prior to burial. Equivalent dose (De) determinations were made on sets of 24 aliquots using the single aliquot regenerative dose (SAR) OSL protocol. Different permutations of the assimilation of equivalent doses to obtain the burial dose were considered, including weighted combinations and statistical dose models (see Guérin et al., 2017). Dose rates to these sediments were assessed using a combination of low-level environmental radioactivity measurements in the laboratory, and determinations of radionuclide concentrations by mass spectrometry.

Radionuclide concentrations and Environmental dose rates. Radionuclide concentrations of ^{232}Th, ^{238}U and ^{40}K were determined from inductively coupled plasma mass spectrometry (ICP-MS; U, Th) and inductively coupled plasma optical emission spectrometry (ICP-OES; K) at X-Ray Mineral Services, Welshpool (formerly Chemostrat) (Table S9). Infinite matrix dose rates were calculated from these using the conversion factors of Guérin et al. (2011) and adjusted for attenuation by grain size and chemical etching using the datasets of Guérin et al. (2012) and Bell (1979) respectively (Table S10). Low-level environmental radioactivity measurements were also undertaken using a MiDose Solutions µDose unit (S/N 016: Tudyka et al., 2018; Kolb et al., 2022). α and β counts, together with the pulse pairs arising from the subsequent decay chains of 214Bi/214Po, 220Rn/216Po, 212Bi/212Pi and 219Rn/215Po, are used to calculate 238U, 235U, 232Th and 40K specific activities. Three reference standards produced by the International Atomic Energy Agency (IAEA) – IAEA-RGU-1, IAEA-RGTh-1 and IAEA-RGK-1, were used to calibrate the µDose using the methodology of Tudyka et al. (2018). Sample measurements were interleaved with background measurements and measurements of the MiDose Solutions reference material, which is comprised of equal quantities of the 3 reference standards. Sub-samples were presented for measurement in the same geometry as the calibration standards. Count times varied from ~ 170 to 250 ks. These estimates of beta and gamma dose rate were combined using weighted statistics with the infinite matrix dose rates obtained from ICP-MS and ICP-OES.

Water contents as received were measured for all samples in the laboratory: fractional water contents were in the range 10.6 to 25.1 % (mean, 18.8%) and saturated water contents, 18.0 to 24.7 % (mean, 20.8 %). Working values of 9.6-25.1% were adopted to determine effective environmental dose rates (Ḋ). The dry infinite matrix dose rates measurements were used in combination with the assumed burial water contents to determine the total effective dose rates for age estimation (Table S11). The contribution from the cosmic dose ($\dot{D}_{cosmic}$) was determined following Prescott and Hutton (1994), which includes corrections for longitude, latitude and altitude, and the thickness of overburden.

U concentrations ranged between 0.5 and 74 ppm, with a mean of 5.8 ± 0.1 ppm (here and elsewhere, error expressed as standard deviation). Th concentrations ranged between 1.4 and 2.5

ppm, with a mean of 1.8 ± 0.4 ppm. K concentrations between 0.6 and 0.9, with a mean of 0.8 ± 0.1 %. These concentrations are comparable to those observed for VC03, VC07 and VC26: U, 0.5 to 0.8 ppm; Th, 0.9 to 2.7 ppm; and K, 0.4 to 1.2 %.

Dry infinite matrix beta dose rates ranged from 0.6 to 0.8 mGy a^{-1}, with a mean value of 0.70 ± 0.07 mGy a^{-1}, and gamma dose rates between 0.3 and 0.4 mGy a^{-1}, with a mean of 0.34 ± 0.03 mGy a^{-1}. These estimates are similar to those derived from K, U and Th for VC03, VC07 and VC26: beta dose rates of between 0.4 to 1.0 mGy a^{-1}, with a comparable mean 0.7 ± 0.2 mGy a^{-1}; gamma dose rates of 0.2 to 0.4 mGy a^{-1}, with a mean of 0.4 ± 0.1 mGy a^{-1}.

Table S9: ICP-MS and ICP-OES determinations of K (%), U and Th (ppm) concentrations

Core	CERSA#	Depth in core /cm	K / %	U / ppm	Th / ppm
VC04	1574	152	0.63 ± 0.03	0.46 ± 0.02	1.46 ± 0.07
VC05	1575	150	0.85 ± 0.04	0.48 ± 0.02	1.69 ± 0.08
VC06	1576	125	0.79 ± 0.04	0.60 ± 0.03	1.72 ± 0.09
VC06	1577	170	0.74 ± 0.04	0.72 ± 0.04	1.68 ± 0.08
VC24	1578	100	-	-	-
VC24	1579	158	0.73 ± 0.04	0.74 ± 0.04	2.49 ± 0.12
VC25	1580	185	0.85 ± 0.04	0.46 ± 0.02	1.52 ± 0.08

Table S10: Infinite matrix dose rates determined from ICP-MS and ICP-OES

Core	CERSA#	Depth in core /cm	ICP-OES and ICP-MS			µDOSE	
			Alpha, dry /mGy a^{-1}	Beta, dry /mGy a^{-1}	Gamma, dry /mGy a^{-1}	Beta, dry /mGy a^{-1}	Gamma, dry /mGy a^{-1}
VC04	1574	152	2.37 ± 0.08	0.57 ± 0.03	0.28 ± 0.01	0.47 ± 0.05	0.21 ± 0.02
VC05	1575	150	2.60 ± 0.09	0.75 ± 0.03	0.35 ± 0.01	0.68 ± 0.05	0.30 ± 0.02
VC06	1576	125	2.95 ± 0.11	0.72 ± 0.03	0.35 ± 0.01	0.61 ± 0.05	0.31 ± 0.02
VC06	1577	170	3.26 ± 0.12	0.70 ± 0.03	0.35 ± 0.01	0.57 ± 0.05	0.29 ± 0.02
VC24	1578	100	-	-	-	-	-
VC24	1579	158	3.9 ± 0.14	0.71 ± 0.03	0.38 ± 0.01	0.60 ± 0.05	0.35 ± 0.02
VC25	1580	185	2.42 ± 0.09	0.75 ± 0.03	0.34 ± 0.01	0.71 ± 0.05	0.28 ± 0.02

Table S11: Total environmnetal dose rates: [a]Effective beta dose rate combining water content corrections with inverse grain size attenuation factors obtained Mejdahl (1979) for K, U, and Th; [b] gamma dose rates reconciled using a distance-weigthed contribution; [c]includes a cosmic dose contribution

Core	CERSA#	Depth in core /cm	Water content	Cosmic dose $\dot{D}_{cosmic}$ / mGy a^{-1}	Beta $\dot{D}_{\beta}$ / mGy a^{-1}	Gamma $\dot{D}_{\gamma}$ / mGy a^{-1}	Total dose $\dot{D}_{eff}$ / mGy a^{-1}
VC04	1574	152	16 ± 5	0.15 ± 0.02	0.46 ± 0.03	0.22 ± 0.01	0.82 ± 0.03
VC05	1575	150	20 ± 6	0.15 ± 0.01	0.59 ± 0.03	0.26 ± 0.01	1.00 ± 0.04
VC06	1576	125	25 ± 8	0.15 ± 0.02	0.52 ± 0.03	0.26 ± 0.04	0.93 ± 0.06
VC06	1577	170	21 ± 6	0.14 ± 0.01	0.52 ± 0.03	0.26 ± 0.04	0.92 ± 0.06
VC24	1578	100	18 ± 5	0.16 ± 0.02	0.55 ± 0.03	0.31 ± 0.01	1.00 ± 0.04
VC24	1579	158	18 ± 5	0.15 ± 0.01	0.55 ± 0.03	0.31 ± 0.01	1.01 ± 0.04
VC25	1580	185	21 ± 6	0.14 ± 0.01	0.59 ± 0.03	0.25 ± 0.01	0.98 ± 0.04

Equivalent dose determinations and distribution analysis. The equivalent dose distributions are shown in figures S4 and S5: figure S4 shows the luminescence stratigraphies for TP22-VC06-1 and TP22-VC05, western and central transects, whereas figure S5 shows the luminescence stratigraphies for TP22-VC24, TP22-VC25 and TP22-VC04, eastern transect. For age assimilation below, the **weighted mean** and standard deviation of the distribution were used in determining depositional ages.

Age assimilations. Table S12 lists the burial doses, environmental dose rates and corresponding depositional ages for CERSA1574-1580.

Table S12: Burial doses, total effective environmental dose rates and corresponding depositional ages.

Core	***CERSA#***	***Depth / cm***	**Palaeodose / Gy**	**Aliquots, n**	**Dose rate / mGy a^{-1}**	**Age / ka**	**Calendar years**
VC04	1574	152	0.17 ± 0.03	17 (24)	0.82 ± 0.03	0.20 ± 0.03	1820 ± 30 CE
VC05	1575	150	0.72 ± 0.05	19 (24)	1.00 ± 0.04	0.72 ± 0.06	1300 ± 60 CE
VC06	1576	125	1.12 ± 0.04	17 (24)	0.93 ± 0.06	1.20 ± 0.09	820 ± 90 CE
VC06	1577	170	91.0 ± 31.5	22 (24)	0.92 ± 0.06	98.6 ± 34.7	
VC24	1578	100	0.43 ± 0.13	17 (24)	1.00 ± 0.04	0.43 ± 0.13	1600 ± 130 CE
VC24	1579	158	1.33 ± 0.06	19 (24)	1.01 ± 0.04	1.32 ± 0.08	700 ± 80 CE
VC25	1580	185	0.43 ± 0.03	22 (24)	0.98 ± 0.04	0.44 ± 0.03	1580 ± 30 CE

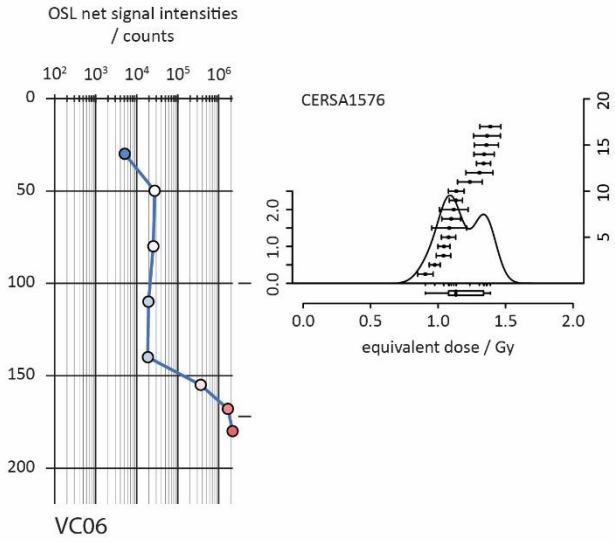

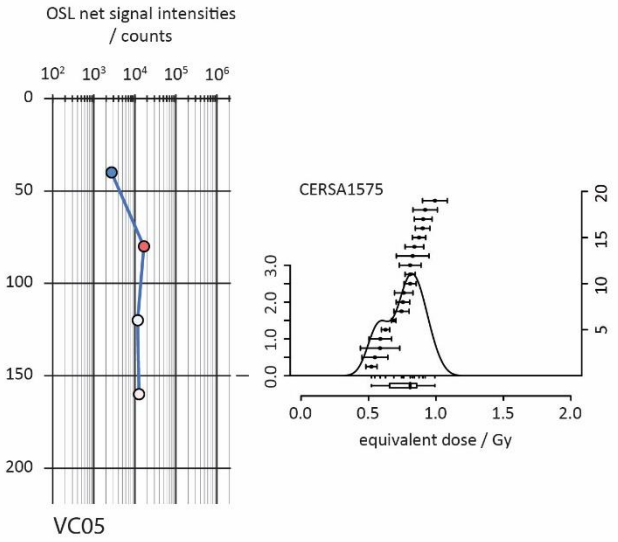

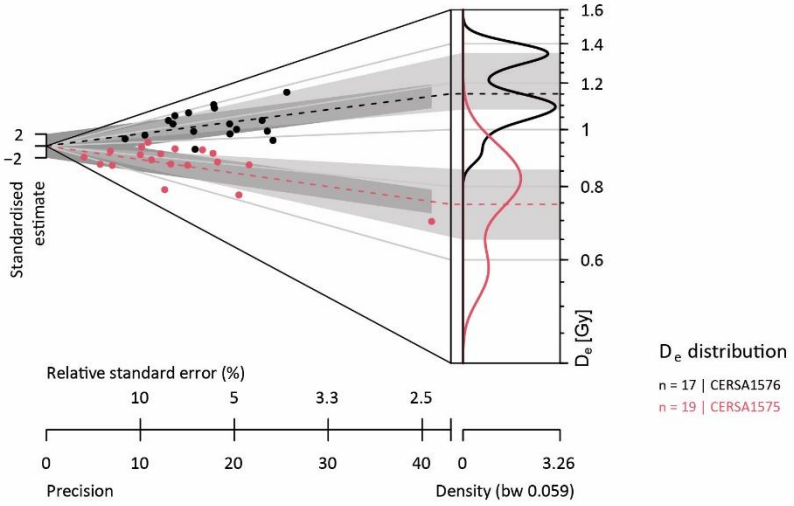

Figure S4: Equivalent dose distributions for CERSA1576 (TP22-VC06-1, western transect) and CERSA1575 (TP22-VC05, central transect) as individual kernel density estimate plots and a combined Abanico Plot.

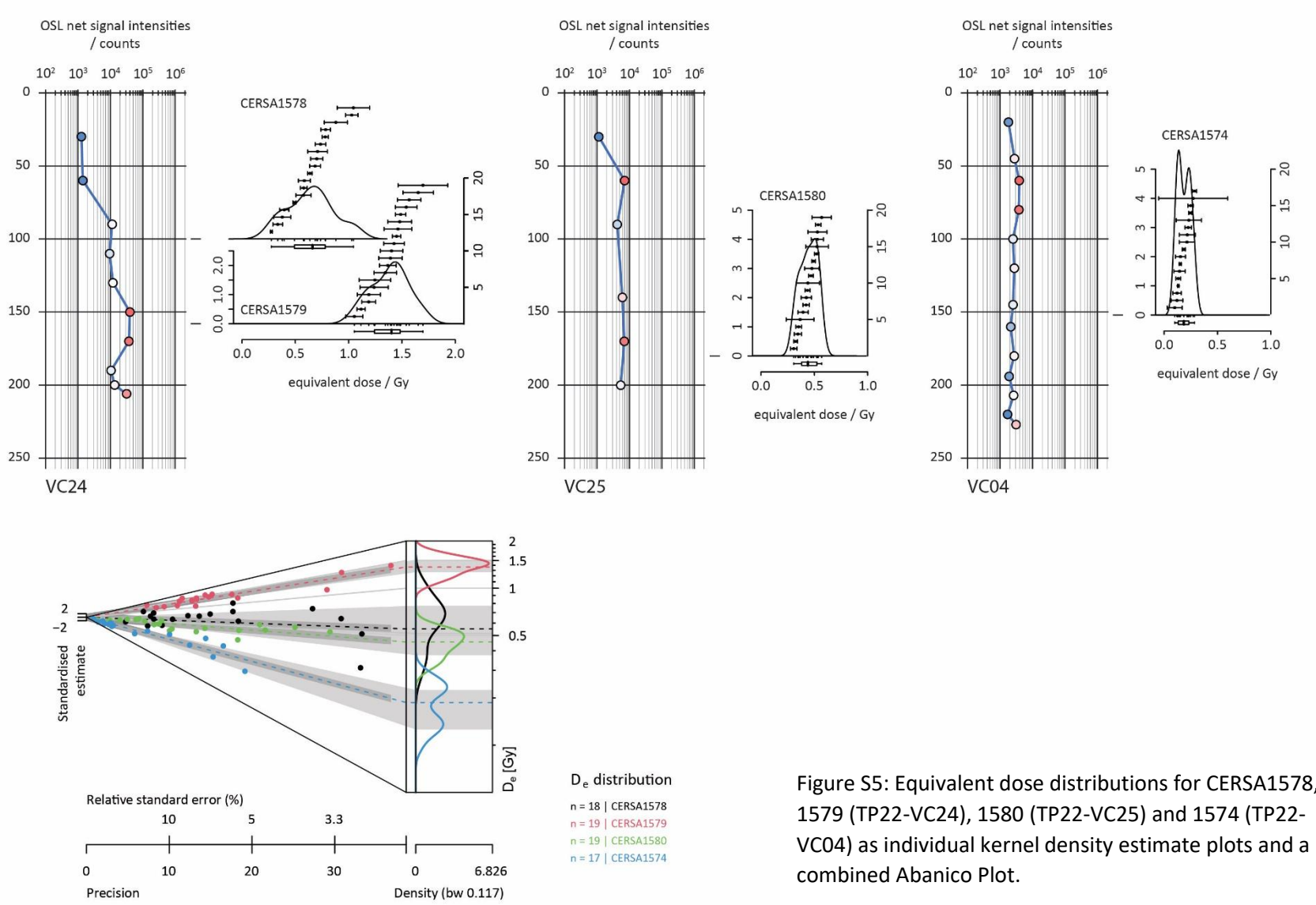

Figure S5: Equivalent dose distributions for CERSA1578, 1579 (TP22-VC24), 1580 (TP22-VC25) and 1574 (TP22-VC04) as individual kernel density estimate plots and a combined Abanico Plot.

References

Bell, W.T., 1979. Attenuation factors for the absorbed radiation dose in quartz inclusions for thermoluminescence dating. Anc. TL 8, 1–12. https://doi.org/10.26034/la.atl.1979.022

Guérin, G., Christophe, C., Philippe, A., Murray, A.S., Thomsen, K.J., Tribolo, C., Urbanová, P., Jain, M., Guibert, P., Mercier, N., Kreutzer, S., Lahaye, C., 2017. Absorbed dose, equivalent dose, measured dose rates, and implications for OSL age estimates: introducing the Average Dose Model. Quat. Geochronol. 41, 163–173. https://doi.org/10.1016/j.quageo.2017.04.002

Guérin, G., Mercier, N., Adamiec, G., 2011. Dose-rate conversion factors: update. Anc. TL 29, 5–8. https://doi.org/10.26034/la.atl.2011.443

Guérin, G., Mercier, N., Nathan, R., Adamiec, G., Lefrais, Y., 2012. On the use of the infinite matrix assumption and associated concepts: a critical review. Radiat. Meas. 47, 778–785. https://doi.org/10.1016/j.radmeas.2012.04.004

Kolb, T., Tudyka, K., Kadereit, A., Lomax, J., Poręba, G., Zander, A., Zipf, L., Fuchs, M., 2022. The µDose system: determination of environmental dose rates by combined alpha and beta counting – performance tests and practical experiences. Geochronology 4, 1–31. https://doi.org/10.5194/gchron-4-1-2022

Mejdahl, V., 1979. Thermoluminescence dating: beta-dose attenuation in quartz grains. Archaeometry 21, 61–72. https://doi.org/10.1111/j.1475-4754.1979.tb00241.x

Prescott, J.R., Hutton, J.T., 1994. Cosmic ray contributions to dose rates for luminescence and ESR dating: large depths and long-term time variations. Radiat. Meas. 23, 497–500. https://doi.org/10.1016/1350-4487(94)90086-8

Tudyka, K., Miłosz, S., Adamiec, G., Bluszcz, A., Poręba, G., Paszkowski, Ł., Kolarczyk, A., 2018. µDose: a compact system for environmental radioactivity and dose rate measurement. Radiat. Meas. 118, 8–13. https://doi.org/10.1016/j.radmeas.2018.07.016